

Role of Functionalized Graphene Quantum Dots in Hydrogen Evolution Reaction: A Density Functional Theory Study

Vaishali Sharma^{1,*}, Basant Roondhe², Sumit Saxena² and Alok Shukla^{1,*}

¹*Department of Physics, Indian Institute of Technology Bombay, Powai, Mumbai 400076, India*

²*Nanostructures Engineering and Modeling Laboratory, Department of Metallurgical Engineering and Materials Science, Indian Institute of Technology Bombay, Mumbai, MH 400076, India*

*Corresponding author email: oshivaishali@gmail.com, shukla@phy.iitb.ac.in

Abstract: Rapid advances in the field of catalysis require a microscopic understanding of the catalytic mechanisms. However, in recent times, experimental insights in this field have fallen short of expectations. Furthermore, experimental searches of novel catalytic materials are expensive and time-consuming, with no guarantees of success. As a result, density functional theory (DFT) can be quite advantageous in advancing this field because of the microscopic insights it provides and thus can guide experimental searches of novel catalysts. Several recent works have demonstrated that low-dimensional materials can be very efficient catalysts. Graphene quantum dots (GQDs) have gained much attention in past years due to their unique properties like low toxicity, chemical inertness, biocompatibility, crystallinity, etc. These properties of GQDs which are due to quantum confinement and edge effects facilitate their applications in various fields like sensing, photoelectronics, catalysis, and many more. Furthermore, the properties of GQDs can be enhanced by doping and functionalization. In order to understand the effects of functionalization by oxygen and boron based groups on the catalytic properties relevant to the hydrogen-evolution reaction (HER), we perform a systematic study of GQDs functionalized with the oxygen (O), borinic acid (BC₂O), and boronic acid (BCO₂). All calculations that included geometry optimization, electronic and adsorption mechanism, were carried out using the Gaussian16 package, employing the hybrid functional B3LYP, and the basis set 6-31G(d,p). With the variation in functionalization groups in GQDs, we observe significant changes in their electronic properties. The adsorption energy E_{ads} of hydrogen over O-GQD, BC₂O-GQD, and BCO₂-GQD is -0.059 eV, -0.031 eV and -0.032 eV respectively. Accordingly, Gibbs free energy (ΔG) of hydrogen adsorption is extraordinarily near the ideal value (0 eV) for all the three types of functionalized GQDs. Thus, the present work suggests pathways for experimental realization of low-cost and multifunctional GQDs based catalysts for clean and renewable hydrogen energy production.

Keywords: Hydrogen evolution reaction; graphene quantum dots; functionalization; density functional theory; overpotential

Introduction

Continuous increase in the consumption of fossil fuels to fulfill ever-increasing energy needs of humanity has led to enormous pollution and degradation of the environment. This has prompted a worldwide effort by researchers to explore novel clean and renewable energy sources. The research has suggested hydrogen to become the first-choice fuel, with the potential to replace fossil fuels, due to its abundance in nature, high energy density, and most importantly its environmental friendliness [1-2]. Several methods have been developed for producing hydrogen of which electrochemical water splitting has demonstrated great promise because of its high hydrogen production efficiency, purity and above all absence of other greenhouse gases or pollutant production in the process [3]. The half reactions for water-splitting, the hydrogen evolution reaction (HER) is difficult to conduct unless the process is assisted by an active catalyst to effectively minimize the required overpotential which is the main concern. From past decades, electrocatalysis studies have received active attention by both experimental as well as computational groups [3] because of their possible applications in developing renewable and clean energy through energy harvesting. The economic feasibility of electrocatalytic water splitting is crucial and can be achieved by decreasing both the energetic cost (i.e., overpotential) and the material cost for the two half-reactions, the oxygen evolution reaction (OER) and the hydrogen evolution reaction (HER) [4-6]. Nano-sized materials can be quite efficient as catalysts due to their significant advantages such as low fabrication cost and high specific surface area to reach the surface reaction area. Generally, Pt-based materials have been regarded as the most effective catalysts for HER [7-8], however, they cannot be used widely and practically due to their scarcity and high cost. Therefore, there is an urgent need to develop inexpensive alternatives with high HER catalytic activity. To date, some relatively inexpensive HER catalysts have been investigated

[9–22] such as transition-metal sulfides and phosphides [9-10], pnictides [11], borides [12], carbides [13-14], nitrides [15-16], as well as carbon materials [17-20], and metal–organic complexes [21-22].

Carbon quantum dot (CQDs) have attracted tremendous attention in the past decade due to their potential in bio-imaging [23-24], photodetectors [25], photocatalysis [26-28] and energy related applications [29]. Generally, CQDs including carbon nanodots [30] and graphene QDs (GQDs) [31] have multifold advantages, such as facile synthesis and excellent chemical inertness. Most importantly, GQDs are graphene fragments with desirable optical and electronic properties. Graphene has shown high electron mobility along with superior mechanical and thermal stability making it suitable for many applications, [32-34] but the key deficiency in graphene is its zero band gap which limits its applications in photonics and optoelectronics. Scientists have proposed many approaches by which a band gap can be opened in graphene. One of the effective and largely adopted methods is by reducing the dimensions of graphene into GQDs. The band gap of GQDs can be made to vary from 0-6 eV by: (a) adjusting their shapes and sizes, and (b) by attaching suitable functional groups or ad-atoms [26]. The edge chemistry, surface, and size of GQDs can be effortlessly changed in a very wide range by utilizing different synthesis approaches and subsequent treatments. Among all methods used to tailor electronic properties of GQDs, heteroatom doping is a very effective strategy to alter the electronic properties of nanomaterials [35]. Recently, GQDs with transition metal nanoparticles adsorbed on their surface have been used in hydrolysis for effective hydrogen evolution [36]. Introduction of various heteroatoms results in enhanced catalytic activity due to the fact that they can intensely alter the local spin or charge distribution by carrying an uneven charge distribution in the material [37]. There are several reports on various types of heteroatom doped GQDs like nitrogen (N) doping which is broadly used to tune the typical properties of GQDs as the nitrogen atom has five valence

electrons with a similar atomic radius to the carbon atom. Apart from N, the boron (B) atom also has a similar atomic radius which makes it relatively easy to bond with carbon leading to negligible structural disorder. As a result, B doping of GQDs has attracted significant research interest for its novel properties [38-43]. Additionally, the fabrication method depends on the use of strong oxidizing agents which results in the unavoidable introduction of oxygen-containing functional groups attached to GQDs. These mainly include carboxyl ($-\text{COOH}$), epoxy ($-\text{O}-$), carbonyl ($-(\text{CO})-$), ether ($-\text{OCH}_3$), and hydroxyl ($-\text{OH}$) groups [44]. These attached oxygen containing functional groups significantly enhance the solubility and also alter the electronic and optical properties of GQDs. Thus, making it interesting to see its effect on the HER activity of GQDs. Nevertheless, there is a lack of understanding of the electronic and HER properties of boron and oxygen functionalized GQDs. In this work, we aim to probe the influence of functionalization on the HER activities of GQDs. However, there is a lack of understanding in how the electronic and HER properties of boron and oxygen functionalized GQDs change. In this work, we undertake systematic first-principles DFT to study the effects of three types of chemical configurations containing B and O atoms in the form of borinic acid (BC_2O) and boronic acid (BCO_2) and oxygen (O) functional groups, on the electronic and catalytic properties of GQDs. Our findings will facilitate further and comprehensive exploration of the HER mechanism of B-doped (BC_2O and BCO_2) and O-doped GQDs as a function of doping configurations, thereby providing insights into the design of more efficient GQD based catalytic devices.

Computational Methodology

The geometry optimization and electronic properties calculations were performed using the density functional theory (DFT) as implemented in the Gaussian16 program package [45], along with the B3LYP hybrid exchange-correlation functional. The Gaussian-type split valence basis set 6-31G (p,d), which includes the polarization functions, was employed in the

calculations. For geometry optimization, all considered systems were allowed to relax simultaneously until the gradient forces reached the set threshold value of 0.000450 Hartree/Bohr, RMS force of 0.000300 Hartree/Bohr, maximum displacement of 0.001800 Bohr, and RMS displacement of 0.001200 Bohr. The self-consistent field (SCF) convergence is set to 10^{-8} Hartree. The vibrational frequencies were also evaluated to confirm the absence of imaginary frequencies, in order to ensure the stability of the optimized geometries. Molecular orbitals (MO's) such as highest occupied molecular orbitals (HOMO) and lowest unoccupied molecular orbitals (LUMO) were visualized using with GaussView [46]. The Multiwfn software was employed to generate projected density of states (PDOS) [47]. The adsorption energy was computed using the formula:

$$E_{ads} = E_{system+H_2} - (E_{system} + E_{H_2}) \quad (1)$$

Where $E_{system+H_2}$ denotes total energy of hydrogen molecule over O-GQD/BC₂O-GQD/BCO₂-GQD systems, E_{system} represents optimized total energy O-GQD/BC₂O-GQD/BCO₂-GQD systems and E_{H_2} represents optimized total energy of hydrogen molecule. A negative value of E_{ads} implies a stable adsorption complex on the O-GQD/BC₂O-GQD/BCO₂-GQD systems. Additionally, in order to be sure about the final geometries, we performed one more iteration of geometry optimization (single point calculation) on the system with an adsorbed hydrogen molecule, at the same level of theory. The hydrogen evolution reaction (HER) is an electrochemical reaction consisting of proton reduction at the electrode to initially yield atomic hydrogen, resulting finally in the formation of the H₂ gas. The catalytic surface potential of the considered HER is calculated using the exchange current density linked to the free energy of adsorbed hydrogen (H₂) when the reaction is at equilibrium. The free energy of hydrogen in the adsorbed state can be computed using equation [48]:

$$\Delta G_{H^*} = E_{ads} + \Delta E_{ZPE} - T\Delta S \quad (2)$$

Above, ΔE_{ZPE} denotes zero-point energy (ZPE) corrections (ranging 0.01 eV to 0.04 eV for hydrogen molecule), ΔS denotes entropy difference and T is the temperature. Further, the ΔE_{ZPE} can be written as [49]

$$\Delta E_{ZPE} = E_{ZPE}^{nH} - E_{ZPE}^{(n-1)H} - \frac{1}{2} E_{ZPE}^{H_2} \quad (3)$$

Here, E_{ZPE}^{nH} and $E_{ZPE}^{(n-1)H}$ denote zero-point energy corrections of total energy of the systems with n and $(n - 1)$ hydrogen atoms adsorbed on the catalyst, respectively. $E_{ZPE}^{H_2}$ represents zero-point energy of gas phase H_2 . ΔS in eq. (2) is the entropy variation among gas-phase hydrogen and adsorbed hydrogen which can be evaluated from the H_2 gas entropy [50] using the approximation

$$\Delta S = \left(S_{nH} - S_{(n-1)H} - \frac{1}{2} S_{H_2} \right) \approx \frac{1}{2} S_H^0 \quad (4)$$

Here, S_{nH} is the entropy of the systems with n hydrogen adsorbed and $S_{(n-1)H}$ is the entropy with $n - 1$ hydrogen atoms adsorbed. $\frac{1}{2} S_{H_2}$ is the gaseous phase entropy of hydrogen. S_H^0 is the vibrational entropy of the hydrogen molecule which finally leads to the value of $T S_H^0 = 0.41$ eV [48]. Thus, we finally obtain the working formula:

$$\Delta G_{H^*} = E_{ads} + 0.24 \text{ eV} \quad (5)$$

In order to develop high-quality catalyst for HER, the ideal value of ΔG should be nearly zero because a small $|\Delta G|$ shows superior HER efficacy. ΔG is one of the most significant parameters concerning HER performance of an electrocatalyst. The theory that ideal HER activity of an electrocatalyst should have a ΔG value of around zero was firstly given by Parson and later proved by others [51-54]. If the catalysts bind weakly, it will be problematic for the surface to activate them. However, if the catalysts bind too strongly, it may impede desorption of H_2 molecules by occupying all accessible surface sites, thus making the reaction ineffective. Therefore, for hydrogen evolution reaction, the optimum value of ΔG

should be around zero. Additionally, the other important parameter relevant to HER is the value of E_{ads} , which should be in the vicinity of 0.24 eV. The overpotential (η) can be determined utilizing ΔG :

$$\eta = -\frac{|\Delta G|}{e} \quad (6)$$

Results and Discussion

The strong motivation for the present study arises from the previous studies of oxygen and boron functionalized GQDs [55-56]. In this work, we have considered the functionalization of the GQDs by boron and oxygen by doping them with borinic and boronic acids both of which have B–O bonds, and by the oxygen containing group (O) [57-58]. The three boron- and oxygen-doped geometries considered in this work are shown in Fig. 1. For convenience, oxygen, borinic acid, and boronic acid functionalized GQDs are expressed as O-GQD, BC₂O-GQD and BCO₂-GQD, respectively. Initially, the geometries of O-GQD, BC₂O-GQD and BCO₂-GQD are optimized individually. The optimized structures are presented in Fig. 1. After the optimization, near the attached functional groups, the C-C bond length changes from its standard value 1.42 Å to 1.5 Å in O-GQD, to ~1.48 Å in BCO₂-GQD, and 1.52 Å in BC₂O-GQD, in agreement with previous studies on GQDs [59-63]. The change in C-C bond length strongly depends on the atomic radius of the dopant. For instance, the atoms present in the functional groups considered here (oxygen and boron) have similar bond lengths and atomic radii as carbon, therefore they will attach with the carbon atoms with minimum deformation (with less change in C-C bond length). However, for larger atoms with large atomic radii, it forms sp³-like bonding with C-atoms with noticeable deformation. The B-C bond lengths post-optimization are 1.52 Å, and 1.64 Å for BC₂O-GQD and BCO₂-GQD, respectively, again in good agreement with the earlier work [64]. As seen in Fig. 1, the functionalization in GQDs slightly distorts its hexagonal ring near O, BC₂O and BCO₂ group

which can be due to the inclusion of groups resulting in disruption of sp^2 hybridization transforming to sp^3 hybridization of carbon atoms in GQDs.

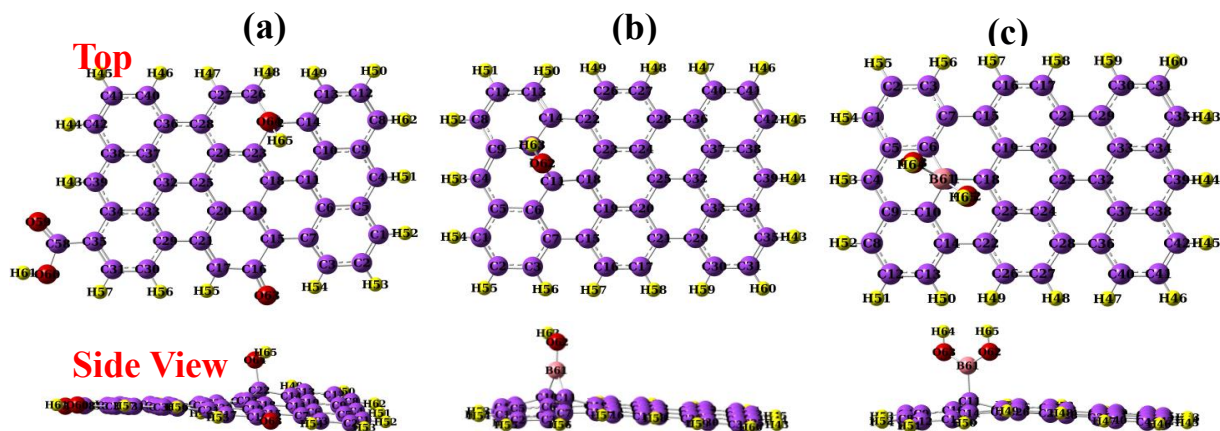


Figure 1: Optimized structures of (a) O-GQD, (b) BC_2O -GQD and (c) BCO_2 -GQD. Yellow, purple, red and pink represent hydrogen, carbon, oxygen and boron atoms, respectively.

This results in a slight pyramid-like structure, i. e. buckling, above the planer structure of the GQDs, again in agreement with the previous studies [65-67]. Next, we re-optimized the geometries with an H_2 molecule adsorbed on top of each functionalized GQD. For the sake of completeness, in Figure 2 we present the initial geometries of O-GQD, BC_2O -GQD and BCO_2 -GQD with a hydrogen (H_2) molecule on top of each structure, before the starting of geometry optimization iterations. In all three cases, the H_2 is placed near the functional groups above the surface, at a distance of 2 Å.

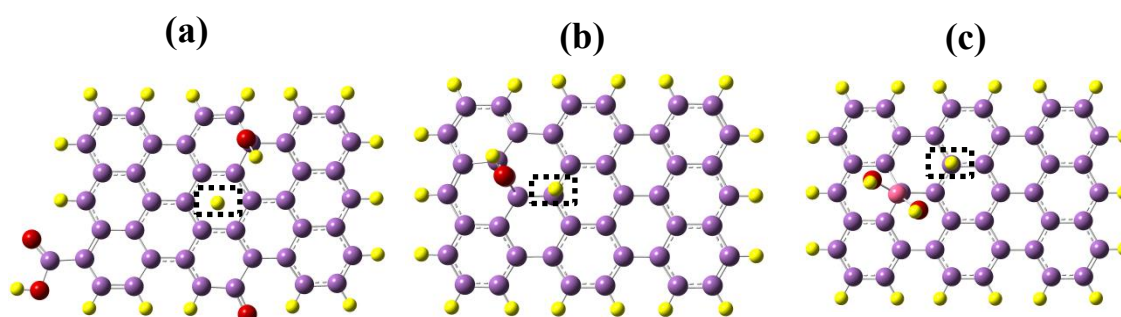


Figure 2: Initial structures of hydrogen over (a) O-GQD, (b) BC_2O -GQD and (c) BCO_2 -GQD. For each GQD, the adsorbed hydrogen molecule is enclosed inside a dashed rectangular box.

Figure 3 shows the optimized structure of H_2 over O-GQD, BC_2O -GQD and BCO_2 -GQD. We also performed vibrational frequency analysis on the final geometries, and the fact that no imaginary frequencies were observed implies that the optimized structures are stable and represent true minima. Following optimization, for H_2 over O-GQD (H_2 -O-GQD), as seen from Fig. 3(a), the hydrogen atom is attracted towards the OH group attached to the ring. The distance of lower hydrogen atom (of hydrogen molecule) with respect to the adjacent carbon changes from 2 Å to 3.7 Å.

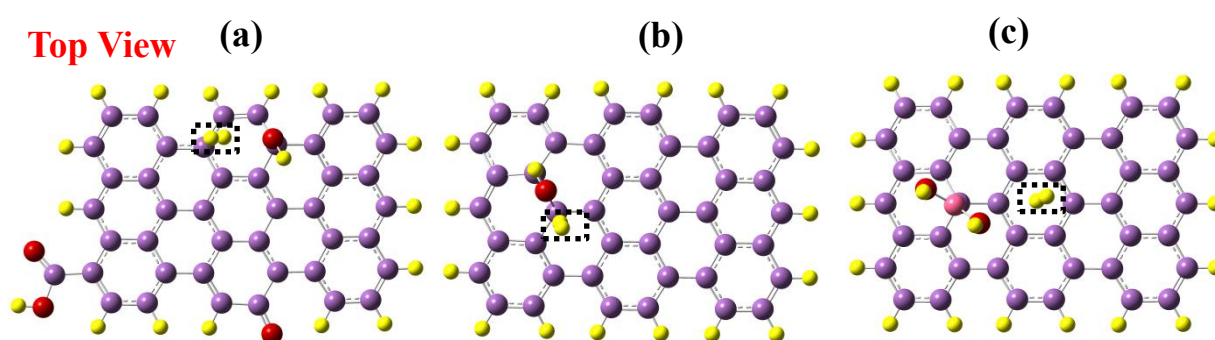


Figure 3: Optimized structures of hydrogen over (a) O-GQD, (b) BC_2O -GQD and (c) BCO_2 -GQD. For each GQD, the adsorbed hydrogen molecule is enclosed inside a dashed rectangular box.

However, the distance between hydrogen and oxygen atom of functional group alters from 2.8 Å to 2.4 Å which is due to the highly electronegative nature of oxygen atom that tends to attract positive charges over hydrogen. For hydrogen over BC_2O -GQD (H_2 - BC_2O -GQD), similar to H_2 -O-GQD, the hydrogen molecule is attracted towards the borinic group, however, H_2 is relocated slightly upward as the distance between hydrogen and oxygen alters to 2.6 Å from 2.3 Å. In case of hydrogen over BCO_2 -GQD (H_2 - BCO_2 -GQD), the H_2 is repelled from its original position and reoriented in the middle of benzene ring of BCO_2 -GQD with C-H (carbon of benzene ring and hydrogen molecule) distance changing to 4.13 Å from 2 Å. The distance between oxygen (oxygen atom of functional group attached) and hydrogen adsorbed slightly increases (from 2.5 Å to 2.6 Å) after optimization. In the adsorbed H_2 molecule, H-H bond distance changes from 0.742 Å to 0.745 Å in the case of

H₂-O-GQD, however, in cases of H₂-BC₂O-GQD and H₂-BCO₂-GQD, it changes to 0.743 Å. Next, the electronic properties of functionalized GQDs considered in this work are analyzed, from the point-of-view of their possible applications as electrocatalysts in HER. The computed dipole moments (p) of various structures are presented in Table 1.

Table 1: Calculated HOMO (E_{HOMO}), LUMO (E_{LUMO}), energy gap (E_g), dipole moment, work function (ϕ) and H-H bond lengths in all the considered systems.

System	E_{HOMO} (eV)	E_{LUMO} (eV)	E_g (eV)	Dipole moment p (D)	ϕ (eV)	$d_{\text{H-H}}$ (Å)
O-GQD	-4.696	-3.512	1.184	3.738	4.104	-
H ₂ -O-GQD	-4.716	-3.523	1.192	3.625	4.120	0.745
BC ₂ O-GQD	-4.114	-2.653	1.460	2.346	3.384	-
H ₂ -BC ₂ O-GQD	-4.125	-2.665	1.459	2.235	3.395	0.743
BCO ₂ -GQD	-4.107	-2.422	1.684	4.052	3.264	-
H ₂ -BCO ₂ -GQD	-4.114	-2.429	1.684	3.949	3.272	0.743

Dipole moments not only give us information about the polarity of a given molecule, but also about its anisotropy, and reactivity as far as electrocatalysis is concerned. It is obvious from Table 1 that p is reduced in all the three structures, i.e., O-GQD, BC₂O-GQD and BCO₂-GQD subsequent to hydrogen adsorption. The value of p varies from ~2.2 D to 4 D indicating: (a) polar nature of bonding in these systems, and (b) structural and electronic anisotropies. The decrement in p indicates that the adsorption of hydrogen molecule in O-GQD, BC₂O-GQD and BCO₂-GQD leads to the decreased polarity in these systems. Additionally, H₂ adsorption in O-GQD, BC₂O-GQD and BCO₂-GQD induces charge transfer, resulting in the modification of p . It is well known that lower values of p lead to relative stability suggesting that the hydrogen adsorbed GQDs are structurally more stable as compared to the original functionalized GQDs considered here [68].

To further understand the electronic properties of the considered structures, the energies of their highest occupied molecular orbitals (HOMO) and lowest unoccupied molecular orbitals (LUMO) are presented in Table 1, while the orbitals are plotted in Fig. 4.

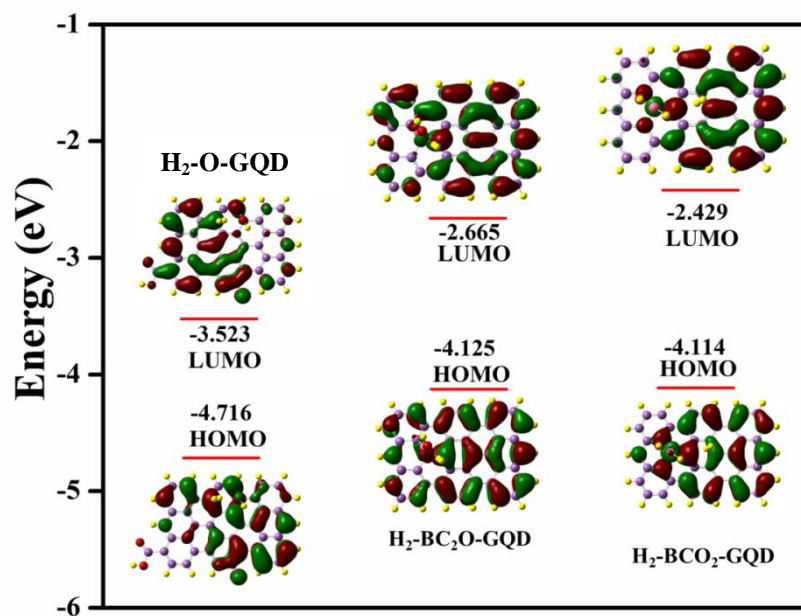


Figure 4: HOMO-LUMO plots of hydrogen over O-GQD, BC₂O-GQD and BCO₂-GQD.

The HOMO levels represent the electron donor properties of the system, and thus show oxidative stability or reactivity of electrophilic kind. The LUMO levels, on the other hand, denote the electron acceptor properties of the system, and, therefore, indicate the reactivity of the nucleophilic kind. In Table 1, we present the energies of the HOMO and LUMO levels along with the band gaps of all the systems considered in this work. From the table, it is obvious that hydrogen over O-GQD, BC₂O-GQD and BCO₂-GQD results in slightly reduced E_{HOMO} values after adsorption depicting their reduced electron-donor ability. Similarly, E_{LUMO} is also reduced depicting their reduced electron-acceptor ability. After the adsorption of the hydrogen molecule, extremely small to no change in the E_g is observed indicating a moderate influence of H₂ adsorption on the band gaps of O-GQD, BC₂O-GQD and BCO₂-GQD. The values of the band gaps E_g of BC₂O-GQD and BCO₂-GQD are in good agreement

with the previously reported work [55]. An efficient electrocatalyst for HER should possess active sites for catalysis. As electrons contribute to HER process, the catalyst should have larger electronic conductivity which depends on the band gap (E_g) in a simple way: the larger the value of E_g , the lower the conductivity and vice versa. From Table 1, it is obvious that H₂-O-GQD has the smallest band gap as compared to the other two H₂ adsorbed GQDs. Therefore, comparatively, we expect it to have the highest electronic conductivity leading to the best electrocatalytic performance in HER [69-71]. Figure 5 presents total and projected density of states (PDOS) of O-GQD, BC₂O-GQD, and BCO₂-GQD, together with and without the adsorbed hydrogen molecule. The PDOS provides the understanding of occupied/unoccupied electronic levels, together with the spatial distribution of particular constituent atoms electronic orbitals. For O-GQD, it can be seen that carbon and oxygen mainly contribute to the HOMO levels, however, hydrogen contributes to LUMO energy levels. Similar behavior is visible in the case of H₂-O-GQD. In case of BC₂O-GQD, the contribution of carbon is solely to the HOMO level, while, hydrogen, boron and oxygen provide larger contributions to the LUMO level. Furthermore, in H₂-BC₂O-GQD, oxygen also makes significant contributions in the HOMO region. Additionally, similar PDOS curves are observed in case of BCO₂-GQD and H₂-BCO₂-GQD indicating major contributions of carbon, hydrogen, boron and oxygen atoms to the HOMO levels. It is obvious from the figure (Fig 5 (a-f)) that both TDOS and PDOS are higher in the HOMO region as compared to the LUMO region.

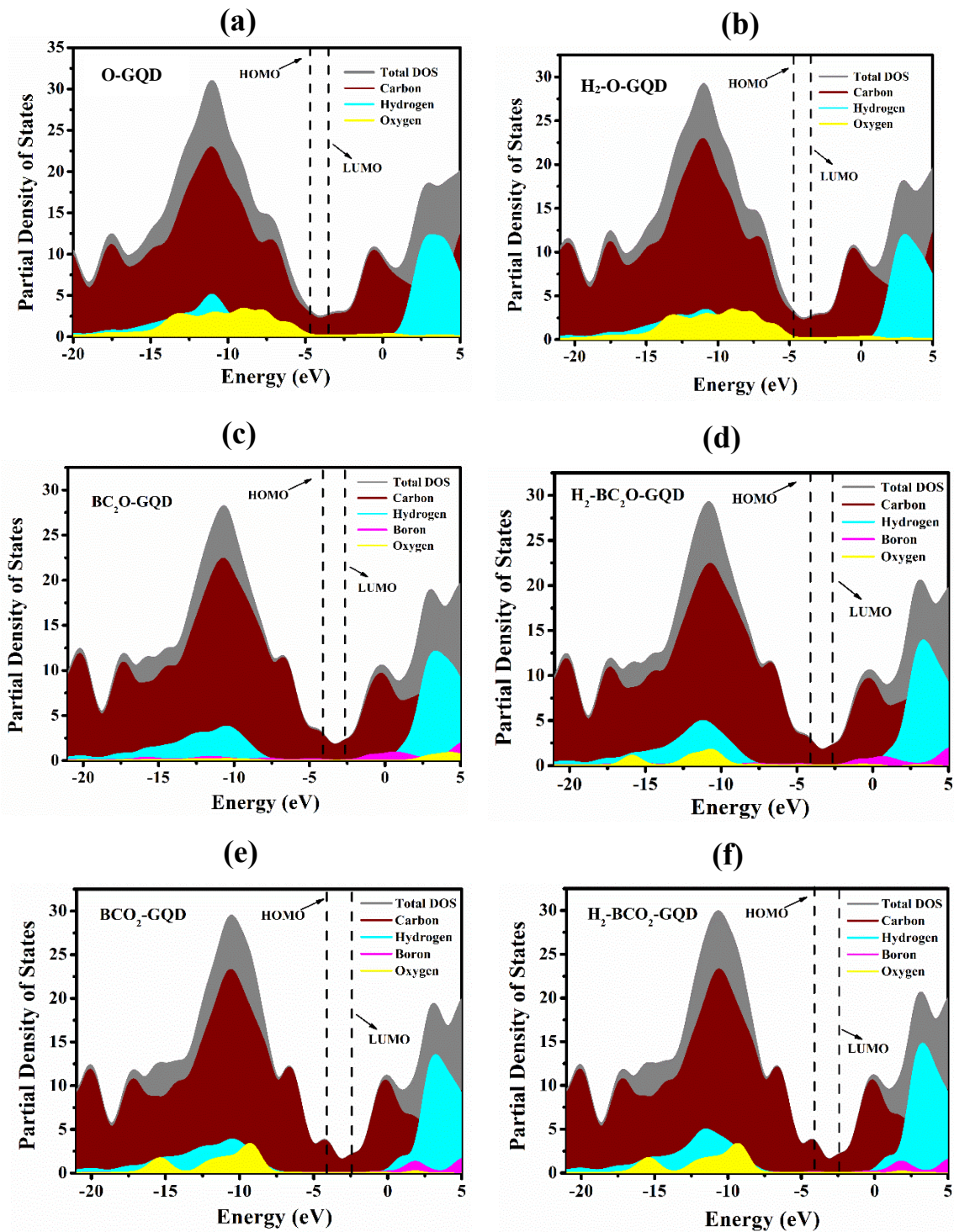


Figure 5: Total and atom projected density of states plots of (a) O-GQD, (b) BC_2O -GQD, (c) BCO_2 -GQD (d) H_2 -O-GQD, (e) H_2 - BC_2O -GQD and (f) H_2 - BCO_2 -GQD.

It is also observed that the DOS plots in all the cases are very similar to each other from which it is evident that different functional groups and adsorbed hydrogen molecules have a

minimal effect on the electronic structure of GQDs. The only changes one notices are small modifications in the positions of HOMO and LUMO energy levels. Thus, it can be said that the electronic structure of the GQDs is affected only near the Fermi level through the orbital hybridization caused by the functional groups, imparting the sp^2 hybridized carbon atoms with a bit of sp^3 character [55]. The work function (ϕ) of a system is the minimum energy required to extract an electron from it to a point in a vacuum immediately outside the surface, without any kinetic energy [72]. Therefore, to attain an understanding of the influence of the adsorbed hydrogen on the reactive properties of O-GQD/BC₂O-GQD/BCO₂-GQD, ϕ has been calculated. For this purpose, the following equation was used:

$$\phi = \frac{\text{Ionization potential} + \text{Electron affinity}}{2} \quad (7)$$

The ionization potential (IP) of a system can be estimated from its HOMO energy as $IP = -E_{HOMO}$, while the electron affinity can be estimated from its LUMO energy as $EA = -E_{LUMO}$ [73]. IP and EA values are significant in examining the electrochemical stability of the considered systems. The calculated values of E_{HOMO} , E_{LUMO} , and ϕ are tabulated in Table 1. It is found that ϕ of all the three structures increases by very small amounts after the hydrogen adsorption. For H₂-O-GQD, when compared to the other structures, we obtain the highest value of the work function 4.120 eV. This also suggests higher stability of H₂-O-GQD, as compared to the other two. Furthermore, our calculated value of ϕ for H₂-O-GQD is quite close to the work functions of Pt and Pd catalysts, suggesting that this system could prove to be an excellent catalyst for HER.

Having discussed the structural and electronic properties of the functionalized GQD systems, subsequently, their HER performances using the Sabatier principle are studied [74]. We consider the H₂ adsorption on O-GQD, BC₂O-GQD and BCO₂-GQD by placing the molecule near the functional groups to understand their contribution to the whole process. The

interaction between H₂ and O-GQD, BC₂O-GQD and BCO₂-GQD is estimated by computing the adsorption energies E_{ads} (eqn. (1)), and the results are presented in Table 2. E_{ads} of H₂ is a significant parameter when analyzing the catalytic activity on the surface of the concerned catalyst. Among O-GQD, BC₂O-GQD and BCO₂-GQD, the highest E_{ads} of -0.059 eV is obtained for H₂-O-GQD. Roughly half of that value, -0.03 eV, is found when it comes to E_{ads} of H₂-BC₂O-GQD and H₂-BCO₂-GQD. For the efficient HER activity, it is important to produce a catalyst that does not attach strongly with the hydrogen in order to make the desorption step attainable, or, else, the objective of the hydrogen energy production will be impossible to fulfill. The calculated values of E_{ads} suggest very feeble interaction of hydrogen with O-GQD, BC₂O-GQD and BCO₂-GQD, suggesting that these structures are good contestants for noble-metal free HER electrocatalysis. Generally, the higher E_{ads} of H₂-O-GQD is the result of higher work function [75]. Next, using the values of work function, we compute the values of open-circuit potential V in an aqueous electrolyte using the equation:

$$V = \frac{\phi}{e} - 4.44 \quad (8)$$

In above equation, 4.44 is the absolute potential value of the standard hydrogen electrode [76]. The open-circuit potential V values for all considered systems are tabulated in Table 2. The value ranges between -0.33 V to -1.16 V following the adsorption of hydrogen molecule. The water electrolysis device comprises anode and cathode as catalysts for HER and oxygen evolution reactions (OER) [77]. For the water-reduction reaction at the cathode, two mechanisms play important roles in the acidic media: (a) the Volmer–Heyrovsky, and (b) Volmer–Tafel mechanisms [77]. Regardless of the route acquired by HER, for both the mechanisms, E_{ads} of hydrogen is an essential parameter defining the catalytic activity on the surface of catalyst. According to the Sabatier principle, the free energy (ΔG) is directly proportional to the exchange current density, which in turn is a measure of catalytic

efficiency [43]. Because ΔG is connected to E_{ads} through Eq. 5, both these quantities can be used to gauge the efficiency of the considered structures as catalysts for HER [78-79]. The values of ΔG of H₂-O-GQD, H₂-BC₂O-GQD and H₂-BCO₂-GQD, calculated using eqn. 5, are presented in Table 2. Along with that, Gibbs free energies of hydrogen evolution reaction are also calculated using thermochemistry analysis. The Gibbs free energies of reaction are calculated employing the formula [80]: $\Delta_r G^\circ(298K) = \sum(\varepsilon_0 + G_{corr})_{product} - \sum(\varepsilon_0 + G_{corr})_{reactants}$

Here, $(\varepsilon_0 + G_{corr})_{product}$ are free energies of H₂-O-GQD/H₂-BC₂O-GQD/H₂-BCO₂-GQD systems, while $(\varepsilon_0 + G_{corr})_{reactants}$ denotes the sum of the free energies of H₂ and O-GQD/BC₂O-GQD/BCO₂-GQD, respectively. The above Σ denotes the sum over different parts of the system (reactant or product), while ε_0 and G_{corr} , respectively, denote the total electronic energy and the correction to the Gibbs free energy due to internal energy, for each part [80].

The values of ΔG of H₂-O-GQD, H₂-BC₂O-GQD and H₂-BCO₂-GQD calculated using this approach are 0.213 eV, 0.183 eV and 0.208, respectively, which are in very good agreement with the values computed using Eq. 5. Figure 6 displays the free-energy diagrams for HER through H₂-O-GQD, H₂-BC₂O-GQD, and H₂-BCO₂-GQD, at 298.15 K. The HER pathway primarily consists of three steps: (a) initial H⁺ + e⁻, (b) an intermediate adsorbed H*, and (c) final production of H₂ molecule [48,81].

Table 2: Calculated adsorption energy (E_{ads}), Gibbs free energy (ΔG), open-circuit potential V and overpotential (η) of all considered systems.

System	ΔE_{ads} (eV)	ΔG (eV)	open-circuit potential V (V)	overpotential η (V)
H ₂ -O-GQD	-0.059	0.181	-0.33	0.181
H ₂ -BC ₂ O-GQD	-0.031	0.209	-1.04	0.209
H ₂ -BCO ₂ -GQD	-0.032	0.206	-1.16	0.206

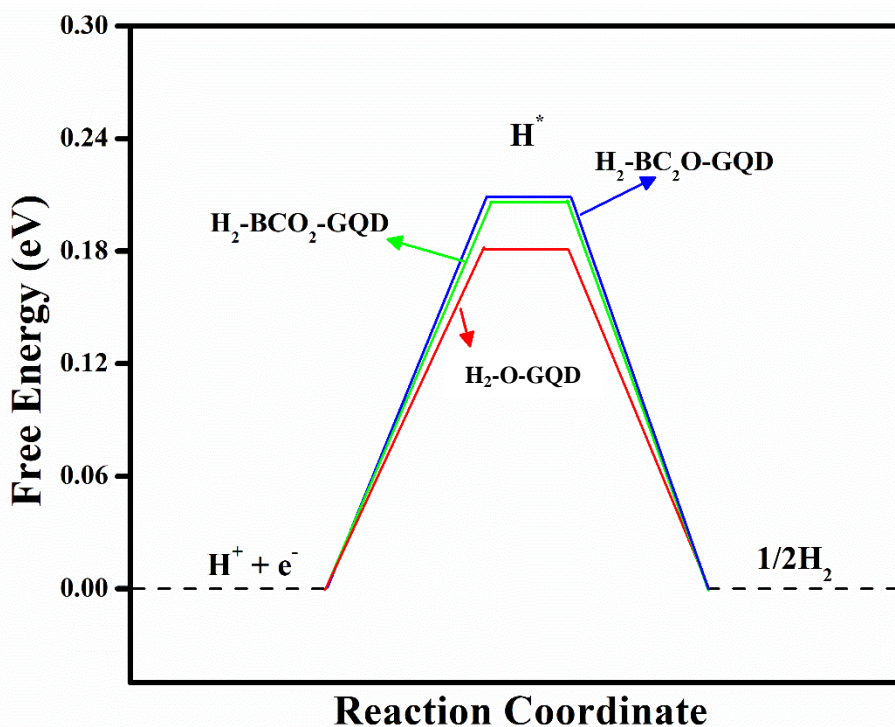


Figure 6: Reaction diagram starting from initial $H^+ + e^-$ and via intermediate adsorbed $2H^*$ resulting in generated H_2 molecules.

Because, the free-energy of adsorption of $2H^*$ is regarded as a better descriptor of the HER activity than that of $1H^*$ [82-83], therefore, we have calculated that quantity, and presented that in Table 2. We note that ΔG (0.181 eV) of H_2 -O-GQD is more favorable as compared to H_2 -BC₂O-GQD (0.209 eV) and H_2 -BCO₂-GQD (0.206 eV). This is attributed to its lower adsorption energy in comparison with the other two systems. As mentioned previously, our calculated value of E_{ads} with O-GQD suggests equivalent HER performance as compared to the palladium and platinum surface [84]. Additionally, H_2 -O-GQD, H_2 -BC₂O-GQD and H_2 -BCO₂-GQD present better HER activity than H monomer over pyrene and coronene polyaromatic hydrocarbons as their binding energy ranges between 0.6–1.6 eV and 0.6–1.4 eV respectively [85].

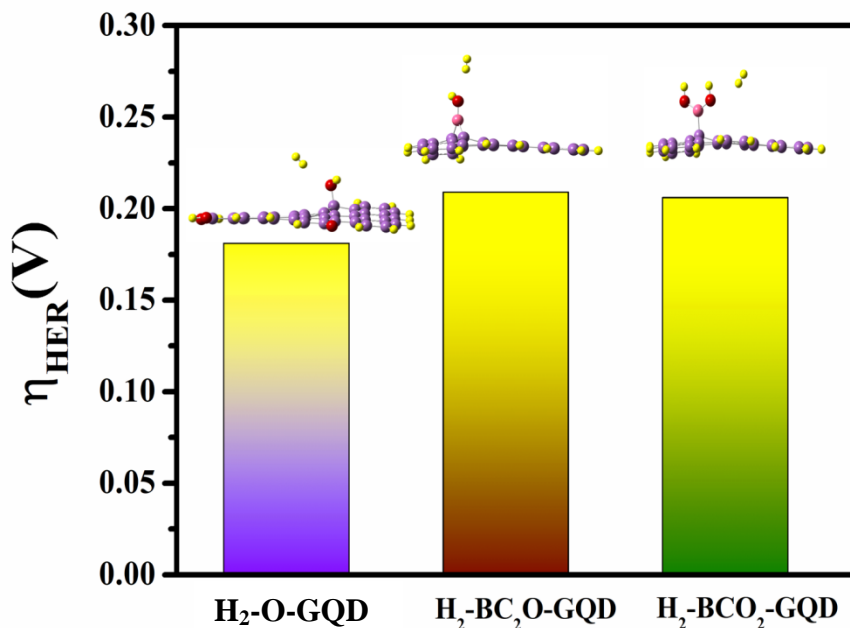


Figure 7: Calculated overpotentials for hydrogen over (a) H₂-O-GQD, (b) H₂-BC₂O-GQD and (c) H₂-BCO₂-GQD.

Using eqn. 6, the overpotential (η) is evaluated and plotted in Fig. 7 for H₂-O-GQD, H₂-BC₂O-GQD and H₂-BCO₂-GQD. Overpotential η is defined as the minimum potential difference between the two electrodes required for starting the electrochemical water-splitting reaction. The role of electrocatalysts is also to lower this η thereby enabling a highly efficient reaction. It is seen from Fig. 7 and Table 2 that H₂-O-GQD has the least value of η (0.181 V), thus, indicating better catalytic activity as compared to H₂-BC₂O-GQD and H₂-BCO₂-GQD. The value of the overpotential for an ideal catalyst for HER is zero, and our calculated values are fairly close to it. Thus, we believe that the structures considered here are strong candidates as catalysts for HER, capable of possibly replacing traditional and costly Pt-based catalysts [86-87].

Conclusion

In present study, functionalized graphene quantum dots are studied using first principles calculations based on density functional theory. The ground state properties, electronic

properties and hydrogen evolution reaction (HER) catalytic activities are examined for oxygen and boron functionalized GQDs (O-GQD, BC₂O-GQD and BCO₂-GQD). The functionalization significantly alters structural and electronic characteristics of GQDs. Our calculations suggest that H₂-O-GQD, with the smallest HOMO-LUMO gap of 1.192 eV compared to other H₂ adsorbed GQDs, will have the best electrocatalytic performance in HER. In pursuit of efficient HER catalyst among the considered systems, adsorption and Gibbs free energy is calculated. The calculated E_{ads} of H₂-O-GQD present superior energies with -0.059 eV value as compared to H₂-BC₂O-GQD and H₂-BCO₂-GQD. Furthermore, as is obvious from the numbers presented in Table 2, the values of other quantities such as adsorption energy, work function, open-circuit potential, overpotential, and the Gibbs free energy of H₂-O-GQD are superior as compared to the corresponding values for other GQDs. The Gibbs free energy of H₂-O-GQD (0.181 eV) is more favorable as compared to H₂-BC₂O-GQD (0.209 eV) and H₂-BCO₂-GQD (0.206 eV). For an ideal catalyst, value of the overpotential for HER is zero, and our calculated values are fairly close to it ranging from 0.18 to 0.2 V. One can always argue that the size of the GQDs considered in this work is not large enough when compared to nanometre sized structures considered in the experiments. In response to that we would like to state that we may not be able to achieve full quantitative agreement with the experiments due to this size difference, but, we strongly believed that our work will provide important qualitative insights and trends which will be useful for the experimentalists. Additionally, we found that the catalytic parameters of H₂-O-GQD are quite comparable to those of Pt and Pd surfaces, which, if true, can have very far-reaching implications in the field. Therefore, we urge the experimentalists to investigate the catalytic performance of the structures considered in this work.

Acknowledgements

Authors VS and BR would like to acknowledge the support by Institute Post-Doctoral Fellowship (IPDF) of the Indian Institute of Technology Bombay.

References

1. Ji M, Wang J. Review and comparison of various hydrogen production methods based on costs and life cycle impact assessment indicators. *Int. J. Hydrog. Energy* 2021;46: 38612-38635.
2. Ishaq H, Dincer I, Crawford C. A review on hydrogen production and utilization: Challenges and opportunities. *Int. J. Hydrog. Energy* 2021. Doi: 10.1016/j.ijhydene.2021.11.149
3. Zhu J, Hu L, Zhao P, Lee LYS, Wong KY. Recent Advances in Electrocatalytic Hydrogen Evolution Using Nanoparticles. *Chem. Rev.* 2020;120:851-918.
4. Lasia A. Mechanism and kinetics of the hydrogen evolution reaction. *Int. J. Hydrog. Energy* 2019;44: 19484-19518.
5. Eftekhari A. Electrocatalysts for hydrogen evolution reaction. *Int. J. Hydrog. Energy* 2017;42:11053-11077.
6. Bhuvanendran N, Ravichandran S, Xu Q, Maiyalagan T, Su H. A quick guide to the assessment of key electrochemical performance indicators for the oxygen reduction reaction: A comprehensive review. *Int. J. Hydrog. Energy* 2022;47:7113-7138.
7. Neto SA, Moreira TFM, Olivi P. Preparation and characterization of active and cost-effective nickel/platinum electrocatalysts for hydrogen evolution electrocatalysis. *Int. J. Hydrog. Energy* 2019;44: 8079-8088.
8. Bai S, Wang C, Deng M, Gong M, Bai Y, Jiang J et al. Surface Polarization Matters: Enhancing the Hydrogen-Evolution Reaction by Shrinking Pt Shells in Pt–Pd–Graphene Stack Structures. *Angew. Chem., Int. Ed.* 2014;53:12120-12124.
9. Gajaria TK, Roondhe B, Dabhi SD, Śpiewak P, Kurzydłowski KJ, Jha PK. Hydrogen evolution reaction electrocatalysis trends of confined gallium phosphide with substitutional defects. *Int. J. Hydrog. Energy* 2020;45: 23928-23936.
10. Chung DY, Park SK, Chung YH, Yu SH, Lim DH, Jung N, et al. Edge-exposed MoS₂ nano-assembled structures as efficient electrocatalysts for hydrogen evolution reaction. *Nanoscale* 2014;6:2131-2136.
11. Gajaria TK, Roondhe B, Dabhi SD, Jha PK. Exploring the hidden catalyst from boron pnictide family for HER and OER. *Int. J. Hydrog. Energy* 2020;45: 18612-18622.
12. Scanlon MD, Bian X, Vrabel H, Amstutz V, Schenk K, Hu X. Low-cost industrially available molybdenum boride and carbide as “platinum-like” catalysts for the hydrogen evolution reaction in biphasic liquid systems. *Phys. Chem. Chem. Phys.* 2013;15:2847-2857 .
13. Li JS, Wang Y, Liu CH, Li SL, Wang YG, Dong LZ et al. Coupled molybdenum carbide and reduced graphene oxide electrocatalysts for efficient hydrogen evolution. *Nat. Commun.* 2016;7:11204.

14. Liu Y, Yu G, Li GD, Sun Y, Asefa T, Chen W, Zou X. Coupling Mo₂C with Nitrogen-Rich Nanocarbon Leads to Efficient Hydrogen-Evolution Electrocatalytic Sites. *Angew. Chem., Int. Ed.* 2015;54:10752-10757.
15. Yan H, Tian C, Wang L, Wu A, Meng M, Zhao L, Fu H. Phosphorus-modified tungsten nitride/reduced graphene oxide as a high-performance, non-noble-metal electrocatalyst for the hydrogen evolution reaction. *Angew. Chem., Int. Ed.* 2015;54: 6325-6329.
16. Chen WF, Sasaki K, Ma C, Frenkel AI, Marinkovic N, Muckerman JT et al. Hydrogen-evolution catalysts based on non-noble metal nickel-molybdenum nitride nanosheets. *Angew. Chem., Int. Ed.* 2012;51:6131-6135.
17. Nemiwal M, Zhang TC, Kumar D. Graphene-based electrocatalysts: Hydrogen evolution reactions and overall water splitting. *Int. J. Hydrog. Energy* 2021;46: 21401-21418.
18. Yang S, Gong Y, Zhang J, Zhan L, Ma L, Fang Z et al. Exfoliated Graphitic Carbon Nitride Nanosheets as Efficient Catalysts for Hydrogen Evolution Under Visible Light. *Adv. Mater.* 2013;25:2452-2456.
19. Sharma V, Kagdada HL, Wang J, Jha PK. Hydrogen adsorption on pristine and platinum decorated graphene quantum dot: A first principle study. *Int. J. Hydrog. Energy* 2020;45:23977-23987.
20. Patel K, Baraiya BA, Som NN, Roondhe B, Jha PK. Investigating hydrogen evolution reaction properties of a new honeycomb 2D AIC. *Int. J. Hydrog. Energy* 2020;45:18602-18611.
21. Wang X, Maeda K, Chen X, Takanabe K, Domen K, Hou Y et al. Polymer Semiconductors for Artificial Photosynthesis: Hydrogen Evolution by Mesoporous Graphitic Carbon Nitride with Visible Light. *J. Am. Chem. Soc.* 2009;131:1680-1681.
22. Qin JS, Du DY, Guan W, Bo XJ, Li YF, Guo LP et al. Ultrastable Polymolybdate-Based Metal-Organic Frameworks as Highly Active Electrocatalysts for Hydrogen Generation from Water. *J. Am. Chem. Soc.* 2015;137:7169-7177.
23. Na N, Liu T, Xu S, Zhang Y, He D, Huang L, Ouyang J. Application of fluorescent carbon nanodots in fluorescence imaging of human serum proteins. *J. Mater. Chem. B* 2013;1:787-792.
24. Dong J, Wang K, Sun L, Sun B, Yang M, Chen H et al. Application of graphene quantum dots for simultaneous fluorescence imaging and tumor-targeted drug delivery. *Sens. Actuators B* 2018;256:616–623.
25. Chiang CW, Haider G, Tan WC, Liou YR, Lai YC, Ravindranath R et al. Highly Stretchable and Sensitive Photodetectors Based on Hybrid Graphene and Graphene Quantum Dots. *ACS Appl. Mater. Interfaces* 2016;8:466–471.
26. Vyas Y, Chundawat P, Dharmendra D, Punjabi PB, Ameta C. Review on hydrogen production photocatalytically using carbon quantum dots: Future fuel. *Int. J. Hydrog. Energy* 2021;46: 37208-37241.
27. Yoon H, Lee K, Kim H, Park M, Novak TG, Hyun G et al. Highly Efficient UV–Visible Photocatalyst from Monolithic 3D Titania/Graphene Quantum Dot Heterostructure Linked by Aminosilane. *Adv. Sustain. Syst.* 2019;3:1900084.

28. Park M, Jeong Y, Kim HS, Lee W, Nam S-H, Lee S et al. Quenching-Resistant Solid-State Photoluminescence of Graphene Quantum Dots: Reduction of π - π Stacking by Surface Functionalization with POSS, PEG, and HDA. *Adv. Funct. Mater* 2021;31: 2102741.
29. Zhang S, Sui L, Dong H, He W, Dong L, Yu L. High-Performance Supercapacitor of Graphene Quantum Dots with Uniform Sizes. *ACS Appl. Mater. Interfaces* 2018;10: 12983–12991.
30. Welsher K, Liu Z, Sherlock SP, Robinson JT, Chen Z, Daranciang D, Dai H, A route to brightly fluorescent carbon nanotubes for near-infrared imaging in mice. *Nat. Nanotechnol.* 2009;4:773-780.
31. Bacon M, Bradley SJ, Nann T. Graphene Quantum Dots. *Part. Part. Syst. Charact.*, 2014;31:415–428.
32. Wang Y, Bao X, Pang B, Zhu Q, Wang J, Zhu D et al. Solution-processed functionalized reduced graphene oxide-an efficient stable electron buffer layer for high-performance solar cells. *Carbon* 2018;131:31–37.
33. Novoselov KS, Geim AK, Morozov SV, Jiang D, Zhang Y, Dubonos SV et al. Electric field effect in atomically thin carbon films. *Science*, 2004;306:666–669.
34. Li Y, Zhao Y, Cheng H, Hu Y, Shi G, Dai L et al. Nitrogen-doped graphene quantum dots with oxygen-rich functional groups. *J. Am. Chem. Soc.* 2012;134:15–18.
35. Zhu P, Wang W, Zhu H, Vargas P, Bont A. Optical Properties of Eu³⁺-Doped Y₂O₃ Nanotubes and Nanosheets Synthesized by Hydrothermal Method. *IEEE Photonics J.* 2018;10:4500210.
36. Shen J, Chen W, Lv G, Yang Z, Yan J, Liu X, Dai Z. Hydrolysis of NH₃BH₃ and NaBH₄ by graphene quantum dots-transition metal nanoparticles for highly effective hydrogen evolution. *Int. J. Hydrog. Energy* 2021;46:796-805.
37. Mahato D, Kharwar YP, Ramanujam K, Haridoss P, Thomas T. S, N co-doped graphene quantum dots decorated TiO₂ and supported with carbon for oxygen reduction reaction catalysis. *Int. J. Hydrog. Energy* 2021;46:21549-21565.
38. Zhang L, Zhang ZY, Liang RP, Li YH, Qiu JD. Boron-doped graphene quantum dots for selective glucose sensing based on the "abnormal" aggregation-induced photoluminescence enhancement. *Anal. Chem.* 2014;86:4423–4430.
39. Tam TV, Kang SG, Babu KF, Oh ES, Lee SG, Choi WM. Synthesis of B-doped graphene quantum dots as a metal-free electrocatalyst for the oxygen reduction reaction. *J. Mater. Chem. A* 2017;5:10537–10543.
40. Chen L, Wu C, Du P, Feng X, Wu P, Cai C. Electrolyzing synthesis of boron-doped graphene quantum dots for fluorescence determination of Fe³⁺ ions in water samples. *Talanta* 2017;164:100–109.
41. Ji L, Chen L, Wu P, Gervasio DF, Cai C. Highly Selective Fluorescence Determination of the Hematin Level in Human Erythrocytes with No Need for Separation from Bulk Hemoglobin. *Anal. Chem.* 2016;88:3935–3944.
42. Chen L, Yang G, Wu P, Cai C. Real-time fluorescence assay of alkaline phosphatase in living cells using boron-doped graphene quantum dots as fluorophores. *Biosens. Bioelectron.* 2017;96:294–299.

43. Yang G, Wu C, Luo X, Liu X, Gao Y, Wu P, Cai C, Saavedra SS. Exploring the Emissive States of Heteroatom-Doped Graphene Quantum Dots. *J. Phys. Chem. C*, 2018, 122, 6483–6492.
44. Li L, Wu G, Yang G, Peng J, Zhao J, Zhu JJ. Focusing on luminescent graphene quantum dots: current status and future perspectives. *Nanoscale* 2013;5:4015–4039.
45. Frisch MJ, Trucks GW, Schlegel HB et al. Gaussian 16, Gaussian, Inc., Wallingford CT, 2016
46. Dennington R, Tod T, Millam J, Eppinett K, Hovell LW, Gilliland R. GaussView; version 6, Semichem Inc.: Shawnee Mission, KS, 2016.
47. Lu T, Chen F. Multiwfn: A Multifunctional Wavefunction Analyzer. *J. Comput. Chem.* 2012;33:580–592.
48. Nørskov JK, Bligaard T, Logadottir A, Kitchin JR, Chen JG, Pandelov S, Stimming U. Trends in the Exchange Current for Hydrogen Evolution. *J. Electrochem. Soc.* 2005;152:J23–J26.
49. Tsai C, Abild-Pedersen F, Nørskov JK. Tuning the MoS₂ Edge-Site Activity for Hydrogen Evolution Via Support Interactions. *Nano Lett.* 2014;14:1381–1387.
50. Atkins P, de Paula J, Keeler J. *Atkins' Physical Chemistry 11e*; Oxford University Press UK, 2018.
51. Parsons R. The rate of electrolytic hydrogen evolution and the heat of adsorption of hydrogen. *Trans. Faraday Soc.* 1958;54:1053–1063
52. Greeley J, Jaramillo TF, Bonde J, Chorkendorff IB, Nørskov JK. Computational high-throughput screening of electrocatalytic materials for hydrogen evolution. *Nat. Mater.* 2006;5:909–913
53. Kibsgaard J, Tsai C, Chan K, Benck JD, Nørskov JK, Abild-Pedersen F, Jaramillo TF. Designing an improved transition metal phosphide catalyst for hydrogen evolution using experimental and theoretical trends. *Energy Environ. Sci.* 2015;8:3022–3029.
54. Hinnemann B, Moses PG, Bonde J, Jorgensen KPN, Nielsen JH, Horch S, Chorkendorff I, Nørskov JK. Biomimetic hydrogen evolution: MoS₂ nanoparticles as catalyst for hydrogen evolution. *J. Am. Chem. Soc.* 2005;127:5308–5309.
55. Feng J, Dong H, Pang B, Chen Y, Yu L, Dong L. Tuning Electronic and Optical Properties of Graphene Quantum Dots by Selective Boronization. *J. Mater. Chem. C* 2019, 7, 237-246
56. Li Y, Shu H, Niu X, Wang J. Electronic and Optical Properties of Edge-Functionalized Graphene Quantum Dots and the Underlying Mechanism. *J. Phys. Chem. C* 2015;119:24950–24957.
57. Lin Z, Waller GH, Liu Y, Liu M, Wong CP. Simple preparation of nanoporous few-layer nitrogen-doped graphene for use as an efficient electrocatalyst for oxygen reduction and oxygen evolution reactions. *Carbon* 2013;53:130–136.
58. Wu F, Xing Y, Li L, Qian J, Qu W, Wen J et al. Facile Synthesis of Boron-Doped rGO as Cathode Material for High Energy Li–O₂ Batteries. *ACS Appl. Mater. Interfaces* 2016;8:23635–23645
59. Raeyani D, Shojaei S, Ahmadi-Kandjani S. Optical graphene quantum dots gas sensors: Theoretical study. *Superlattices and Microstructures* 2018;114:321–330.

60. Osman W, Abdelsalam H, Ali M, Teleb NH, Yahia IS, Ibrahim MA, Zhang Q. Electronic and magnetic properties of graphene quantum dots doped with alkali metals. *J. Mater. Res. Technol.* 2021;11: 1517-1533.
61. Tian P, Tang L, Teng KS, Lau SP. Graphene quantum dots from chemistry to applications. *Mater. Today Chem.* 2018;10:221-258.
62. Abdelsalam H, Elhaes H, Ibrahim MA. First principles study of edge carboxylated graphene quantum dots. *Phys. B: Condens. Matter* 2018;537:77-86.
63. Yu W, Sisi L, Haiyan Y, Jie L. Progress in the functional modification of graphene/graphene oxide: a review. *RSC Adv.* 2020;10:15328-15345.
64. Montejo-Alvaro F, Oliva J, Herrera-Trejo M, Hdz-García HM, Mtz-Enriquez AI. DFT study of small gas molecules adsorbed on undoped and N-, Si-, B-, and Al-doped graphene quantum dots. *Theor. Chem. Acc.* 2019;138:37.
65. Feng J, Dong H, Pang B, Shao F, Zhang C, Yu L, Dong L. Theoretical study on the optical and electronic properties of graphene quantum dots doped with heteroatoms. *Phys. Chem. Chem. Phys.* 2018;20:15244-15252
66. Sharma V, Som NN, Pillai SB, Jha PK. Utilization of doped GQDs for ultrasensitive detection of catastrophic melamine: a new SERS platform. *Spectrochimica Acta Part A: Molecular and Biomolecular Spectroscopy* 2020;224:117352.
67. Sharma V, Jha PK. Enhancement in power conversion efficiency of edge-functionalized graphene quantum dot through adatoms for solar cell applications. *Sol. Energy Mater. Sol. Cells* 2019;200:109908.
68. Kobrak MN, Li H. Electrostatic Interactions in Ionic Liquids: The Dangers of Dipole and Dielectric Descriptions. *Phys. Chem. Chem. Phys.* 2010;12:1922–1932.
69. Zhang Z, Chen K, Zhao Q, Huang M, Ouyang X. Electrocatalytic and photocatalytic performance of noble metal doped monolayer MoS₂ in the hydrogen evolution reaction: A first principles study. *Nano Materials Science* 2021;3:89-94.
70. Xu Q, Li G, Zhang Y, Yang Q, Sun Y, Felser C. Descriptor for Hydrogen Evolution Catalysts Based on the Bulk Band Structure Effect. *ACS Catal.* 2020;10:5042–5048.
71. Dong S, Wang Z. Improving the catalytic activity for hydrogen evolution of monolayered SnSe_{2(1-x)}S_{2x} by mechanical strain. *Beilstein J. Nanotechnol.* 2018;9:1820–1827
72. Lang ND, Kohn W. Theory of Metal Surfaces: Work Function. *Phys. Rev. B* 1971;3:1215.
73. Talmaciu MM, Bodoki E, Oprean R. Global Chemical Reactivity Parameters for Several Chiral Beta-Blockers from the Density Functional Theory Viewpoint. *Clujul Med.* 2016;89:513-518.
74. Greeley J, Jaramillo TF, Bonde J, Chorkendorff I, Nørskov JK. Computational High-Throughput Screening of Electrocatalytic Materials for Hydrogen Evolution. *Nat. Mater.* 2006;5:909–913.
75. Zeradhanin AR, Vimalanandan A, Polymeros G, Topalov AA, Mayrhofer KJJ, Rohwerder M. Balanced Work Function as a Driver for Facile Hydrogen Evolution Reaction—Comprehension and Experimental Assessment of Interfacial Catalytic Descriptor. *Phys Chem. Chem. Phys.* 2017;19:17019–17027.

76. Trasatti S. The Absolute Electrode Potential: An Explanatory Note (Recommendations 1986). *Pure Appl. Chem.* 1986;58:955–966.
77. Coutanceau C, Baranton S, Audichon T. Hydrogen Production from Water Electrolysis. *Hydrogen Electrochemical Production* 2018:17–62.
78. Gao G, O'Mullane AP, Du A. 2d Mxenes: A New Family of Promising Catalysts for the Hydrogen Evolution Reaction. *ACS Catal.* 2017;7:494–500.
79. Zou X, Zhang Y. Noble Metal-Free Hydrogen Evolution Catalysts for Water Splitting. *Chem. Soc. Rev.* 2015;44:5148–5180.
80. <http://gaussian.com/thermo/>
81. Abghoui Y, Skúlason E. Hydrogen Evolution Reaction Catalyzed by Transition-Metal Nitrides. *J. Phys. Chem. C* 2017;121:24036–24045.
82. Sabatier P. *Catalysis in Organic Chemistry*; D. Van Nostrand Company, 1922.
83. Xu H, Cheng D, Cao D, Zeng XC. A Universal Principle for a Rational Design of Single-Atom Electrocatalysts. *Nat. Catal.* 2018;1:339–348.
84. Pašti IA, Gavrilov NM, Mentus SV. Hydrogen adsorption on palladium and platinum overlayers: DFT study. *Adv Phys Chem*, 2011;2011:305634
85. Rasmussen JA, Henkelman G, Hammer B. Pyrene: hydrogenation, hydrogen evolution, and -band model. *J Chem Phys* 2011;134:164703
86. Morales-Guio CG, Stern LA, Hu X. Nanostructured Hydrotreating Catalysts for Electrochemical Hydrogen Evolution. *Chem. Soc. Rev.* 2014;43:6555–6569.
87. Kibsgaard J, Tsai C, Chan K, Benck JD, Nørskov JK, Abild-Pedersen F et al. Designing an Improved Transition Metal Phosphide Catalyst for Hydrogen Evolution Using Experimental and Theoretical Trends. *Energy Environ. Sci.* 2015;8: 3022–3029.